AIAA JOURNAL
Vol. 36, No. 4, April 1998

Vortex Dynamics of Blade–Blade Interaction

Z. X. Yao* and D. D. Liu†
Arizona State University, Tempe, Arizona 85287-6106

A time domain method has been developed for treatments of vortex dynamics in all classes of blade–blade interaction problems. A new vortex impingement condition is introduced to the discrete vortex tracking scheme and was found most effective in handling the vortex–airfoil interaction and the blade–blade interaction (BBI) problems. Present results are verified with all classical solutions and are found in good agreement with almost all existing solutions. The present BBI study concludes that any front blade movement will induce a strong interaction between the wake and the rear blade; hence, it alters drastically the lift response and the wake structure. Any rear blade movement only induces a weak interaction, hence rendering the blade system ineffective.

Nomenclature

a_{ij} = influence coefficients due to vorticity distribution
C_D = drag coefficient
$\bar{C}_D$ = average drag coefficient over one cycle
$\bar{C}_{D_{\alpha^2}}$ = derivative of the average drag coefficient
C_L = lift coefficient
C_{L_s} = steady-state lift coefficient
C_M = moment coefficient
C_P = pressure coefficient; $\Delta C_P = C_{P_{\text{upper}}} - C_{P_{\text{lower}}}$
c = airfoil chord length
d = horizontal distance between two airfoils
h = vertical distance between two airfoils
k = reduced frequency, $\omega c/U_\infty$
$\boldsymbol{n}$ = normal vector of the airfoil surface
$\boldsymbol{r}$ = position vector
T_i = influence coefficient due to trailing-edge vortex
t = true time
$\bar{t}$ = nondimensional time, tU_∞/c
(x_v, y_v) = vortex position normalized by airfoil chord
α = angle of attack
Γ = total circulation
Γ_{TE} = strength of the trailing-edge vortex
Γ_v = strength of the traveling vortex
γ_j = vorticity strength at the jth endpoint
η = propulsive efficiency

I. Introduction

THE problem of vortex/wake flow and its interaction with airfoils or blades has received considerable attention in recent years. (The terms airfoil and blade are considered equivalent and are used interchangeably throughout the present text.) Central to this problem, treatments of unsteady flow and vortex dynamics are of primary interest. This class of problems covers a vast range of modern aeronautical applications. These applications include the canard–wing–wake interaction and wing–tail interaction in aircraft, the blade–wake interaction in helicopter rotors, and the wake cutting and rotor–stator interaction in turbomachinery.[1]

Several vortex-flow models have been introduced in the past for treatments of these problems.[2–8] Other than the classical airfoil wake interaction (AWI; Fig. 1a) problem, two classes of interactions describing different stages of the vortex–airfoil dynamics can be categorized as follows.

1) Vortex–airfoil interaction (VAI; Fig. 1b): An oncoming single vortex, or a group of multiple vortices, passes by or impinges on a single airfoil. VAI is usually called blade–vortex interaction in helicopter terminology. Interaction here refers to the pressures or lift influenced by the interplay between the oncoming vortices and the airfoil.

2) Blade–blade interaction (BBI; Fig. 1c): Interaction here refers to that of two closely placed airfoils in either transient or oscillatory motions, including that of the wake and the rear airfoil. It turns out that, to study the BBI problem, the solution methods for AWI and VAI must be first sufficiently developed. The approach of BBI could be considered as the composite of the AWI and the VAI procedures.

The objective of this paper is to present our continuing study of the last two classes of problems, whereas our AWI studies have been reported in Ref. 8.

Many methods have been developed in the past, and fruitful results were obtained for the AWI problems[3–5,8–12] and the VAI problems.[6–8,13–20] By contrast, much less progress has been achieved in the area of the BBI problems.[21–24] Attempts to solve the BBI problems are mainly hindered by the complex nature of the wake impingement, or the vortex impingement, on the rear blade. The vortex impingement occurs when the vortices created upstream approach the rear blade head-on. If one adopts the inviscid-flow model, the approaching vortex should obey the tangency condition and thus follow the tangential path over or under the airfoil surface. But if the vortex has a weak vorticity and/or a low induced velocity, and if an improper numerical approach is used, then its computed motion would fail to follow the tangential path during its head-on approach. With a few exceptions in the past,[7,20] most approaches in BBI and VAI studies tend to avoid treating the case of the vortex impingement. It is believed that the problem of vortex impingement is the central issue in the vortex dynamics of BBI and therefore deserves careful attention.

In the present work, a time domain method has been developed for treatments of vortex dynamics in all classes of interaction problems. The present method is based on a high-order boundary element method with cubic spline curved panels and linear source and vorticity distributions. The discrete vortex tracking technique in the Lagrangian frame is adopted for handling wakes and free vortices and their interaction with airfoils (or blades). Discrete free vortices with finite cutoff cores are used to represent the wake or the traveling vortices. A general numerical procedure has been established including the special treatment of the vortex impingement problem. A vortex impingement condition is introduced to the formulation so that a self-correction scheme to the vortex trajectory is provided for the case when the vortices approach the airfoil surface. The present procedure is found to be very effective in the treatment of AWI, VAI, and BBI problems.

Computed results of the AWI study and their proper validation with those of Wagner,[25] Theodorsen,[26] and Katz and Maskew[27] can be found in Ref. 8.

In what follows, we only attempt to present the computed results of VAI and BBI. Finally, the mechanism in the thrust generation of

Presented as Paper 94-0737 at the AIAA 32nd Aerospace Sciences Meeting and Exhibit, Reno, NV, Jan. 10–13, 1994; received Sept. 22, 1994; revision received Sept. 19, 1997; accepted for publication Oct. 1, 1997.

*Faculty Research Associate, Department of Mechanical and Aerospace Engineering; currently Advisory Software Engineer, GBIS, IBM, MS9661, Austin, TX 78758.

†Professor, Department of Mechanical and Aerospace Engineering. Associate Fellow AIAA.

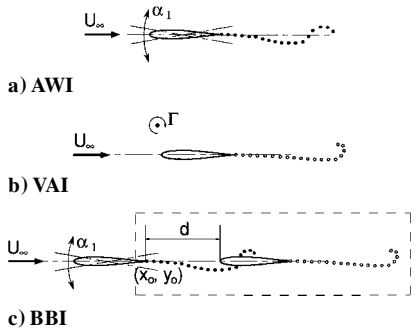

Fig. 1 Basic studies for blade–blade interaction.

Schmidt's wave propeller[28] will be discussed in conjunction with the present results.

II. Theoretical Background

The flow is assumed to be two-dimensional, unsteady, inviscid, and incompressible. In general, the velocity field can be decomposed into a solenoidal velocity field due to the vorticity in the flowfield $\boldsymbol{V}_\omega$ and an irrotational potential velocity field $\boldsymbol{V}_a$, i.e.,

$$\boldsymbol{V} = \boldsymbol{V}_\omega + \boldsymbol{V}_a \tag{1}$$

where $\boldsymbol{V}_\omega$ and $\boldsymbol{V}_a$ should satisfy the flow continuity and the irrotationality condition, respectively.

The potential velocity field $\boldsymbol{V}_a$ for the incompressible flow is obtained by solving the Laplace equation for the velocity potential χ, i.e.,

$$\nabla^2\chi = 0 \qquad \text{where} \qquad \boldsymbol{V}_a = \nabla\chi \tag{2}$$

The solution of this equation can be obtained upon applying Green's third identity.[29]

For an inviscid flow, the boundary condition applied on the body surface is the flow impermeable condition, i.e.,

$$(\boldsymbol{V} - \boldsymbol{V}_s)\cdot\boldsymbol{n} = 0 \tag{3}$$

where $\boldsymbol{V}_S$ is the velocity of the airfoil surface motion.

The total circulation $\Gamma(t)$ in the flowfield is governed by Kelvin's theorem,[30] i.e.,

$$\frac{\mathrm{d}\Gamma(t)}{\mathrm{d}t} = 0 \tag{4}$$

This implies that the total circulation in the flowfield is conserved at all times, i.e.,

$$\Gamma(t) = \text{const} \tag{5}$$

Equation (5) is known as the conservation of vorticity condition.

There exist two different interpretations of the conservation of vorticity condition for VAI studies in the past. Chow and Huang[6] considered that the traveling vortices are generated by the airfoil itself resulting from leading-edge separation as in the dynamic stall problem. Wu et al.[14] and Lee and Smith[7] considered that the traveling vortices are generated from other objects upstream, such as the shed vortices of the front airfoil. The total vorticity contained in Eq. (5) includes the traveling vortices in the former formulation, and it excludes the traveling vortices in the latter. The conservation of vorticity condition is thus termed the internally generated condition and the externally generated condition, respectively, in the present study, following the definitions of Ref. 17.

The unsteady Kutta condition requires no pressure jump across the wake at the airfoil trailing edge, i.e., at the trailing edge,

$$\Delta C_p = 0 \tag{6}$$

Various approaches in the past have implemented this condition in different ways.[3–5] The current method adopts the linearized scheme developed by Kim and Mook.[5] Further discussion on this can be found in Refs. 8 and 31.

III. Numerical Procedure

A high-order panel method developed by Shen and Proft[32] serves as a base for the present unsteady flow development. The airfoil surface is represented by a series of cubic spline curved panels with continuous slopes and curvatures at the panel junctions. A composite of linear source and vorticity distributions is applied on each panel. According to Morino and Kuo,[33] the strengths of the source distributions are predetermined by the slope of the airfoil geometry. The unknown strengths of the vorticity distribution on the airfoil and the strength of the trailing-edge vortex are solved by satisfying the tangency boundary condition, Eq. (3), on the control point of each panel, i.e.,

$$\sum_{j=1}^{N+1} a_{ij}\gamma_j + T_i\Gamma_{\mathrm{TE}} = C_i \tag{7}$$

where N is number of panels and C_i represents the net induced normal velocity at the ith control point due to the source distributions, traveling vortices, wake vortices, and airfoil motion.

Equations (5–7) are solved simultaneously to yield the vorticity strengths of the airfoil elements and the trailing-edge vortex. For VAI and AWI, these equations can be recast into the following matrix form:

$$[A]\{\gamma\} = \{C\} \tag{8}$$

where $[A]$ is the aerodynamic influence coefficient (AIC) matrix for the vorticity distributions, $\{\gamma\} = \{\gamma_j, \Gamma_{\mathrm{TE}}\}^T$ is the array of unknown strengths, and $\{C\}$ is the array of the net induced normal velocities at the control points.

For the BBI, the matrix form of the system of equations is generalized to

$$\begin{bmatrix} A^{11} & A^{12} \\ A^{21} & A^{22} \end{bmatrix} \begin{Bmatrix} \gamma^1 \\ \gamma^2 \end{Bmatrix} = \begin{Bmatrix} C^1 \\ C^2 \end{Bmatrix} \tag{9}$$

where A^{IJ} represents the AIC matrix for the Ith airfoil due to the influence from the Jth airfoil, γ^J is the array of the unknown strengths on the Jth airfoil, and C^I represents the array of the net induced normal velocities at the control points on the Ith airfoil. This system is an overdetermined one and is solved by a least-square method.

The current unsteady problem is solved successively in the time domain. At each time step, the system of equations, Eq. (7) or (8), is solved for the unknown vorticity strengths on each panel and the unknown strength of the trailing-edge vortex. A trailing-edge vortex is then generated and is shed from the trailing edge into the wake. For vortex tracking, the positions of these traveling vortices and wake vortices are discretized in time by the Euler method,[34] i.e.,

$$\boldsymbol{r}(t_{k+1}) = \boldsymbol{r}(t_k) + \boldsymbol{V}(t_k)\cdot\Delta t \tag{10}$$

where $\boldsymbol{r}(t_k)$ is the position vector of a vortex at time $t = t_k$, $\boldsymbol{V}(t_k)$ is the induced velocity at the location of the vortex at $t = t_k$, and Δt is the interval of each time step.

As a criterion to guide the vortex trajectory, a vortex impingement condition is introduced. This condition is based on the principle that the vortex can at most slide along the airfoil surface in an inviscid-flow environment. The current procedure regulates and corrects the predicted trajectory of a vortex as it approaches the proximity of the airfoil surface. If the surface of the airfoil is defined as $S(x, y) = 0$, and the current and predicted positions are $\boldsymbol{r}(t_k) = \{x_k, y_{k1}\}$ and $\boldsymbol{r}(t_{k+1}) = \{x_{k+1}, y_{k+1}\}$, respectively, then the condition provides the following procedures.

1) If $S(x_{k+1}, y_{k+1}) > 0$, the predicted position is outside the airfoil surface; then the position predicted by Eq. (10) is the new position for the vortex.

2) If $S(x_{k+1}, y_{k+1}) < 0$, the predicted position is inside the airfoil surface; then the new position must be corrected by the following equation:

$$\boldsymbol{r}(t_{k+1}) = \boldsymbol{r}(t_k) + |\boldsymbol{V}(t_k)|\cdot\Delta t\cdot\boldsymbol{l} \tag{11}$$

where $\boldsymbol{l}$ is the unit vector tangent to the airfoil surface measured from position (x_k, y_k). This procedure is found to be very effective in that it yields stable solutions for all VAI and BBI problems.

Once unknown strengths are solved, the pressure distribution C_P on the airfoil surface and the force and moment coefficients can be obtained according to the definitions given in Refs. 31 and 35.

IV. Results and Discussion

Computed results of VAI and BBI problems are presented in order. For computed studies of AWI and another class of wake-airfoil interaction (WAI), such as oscillatory wakes impinging on airfoils, the reader is referred to Refs. 31 and 35.

Traveling Vortex over Airfoil

In Fig. 2, a symmetric Joukowski airfoil with thickness of $t = 16.9\%$ and a traveling vortex of strength $\Gamma_v = 1.4745$ is used. The traveling vortex is released at a starting position of $(x_v, y_v) = (-0.47748, 0.41777)$ ahead of the stationary airfoil. Note that the internally generated vortex condition is used in the present study according to Ref. 6 for this case. The predicted lift and drag coefficients are in good agreement with Chow and Huang's[6] results. Shown in Fig. 2c are the snapshots of the wake patterns due to a free vortex passing a Joukowski airfoil from below at different time frames. Although the released position of the free vortex is originated from the upper side of the centerline, the free vortex goes around the airfoil leading edge toward the lower side of the airfoil. Drastic interaction can be seen between the free vortex and the wake as the free vortex passes the trailing edge. Breakup of the wake is caused by the free vortex whose strength is of opposite sign to those of the wake vortices.

Some flow physics can be drawn from our detailed computational studies of this case.

1) The first dip in C_L, which occurred around $\bar{t} \approx 1.80$, is due to the sudden change of the upper and lower surface velocities (hence the sign change in ΔC_P) as induced by the rapid turning of the vortex around the leading edge.

2) Beyond the first C_L dip, the vortex causes the flow to accelerate up to a C_L peak (at $\bar{t} \approx 2.08$). From this peak onward, the flow is decelerated by the vortex motion towards the trailing edge. Drastic vortex/shed-wake interaction renders further reduction in ΔC_P towards a $\Delta C_P = 0$ at the trailing edge (at $\bar{t} \approx 2.24$) as imposed by the Kutta condition. This leads to the second C_L dip.

In Fig. 3, two sets of lift coefficients computed by the present method are compared with those of Wu et al.,[14] McCroskey and Goorjian[15] (Fig. 3a), and Lee and Smith[7] (Fig. 3b). The traveling vortex is released from a position at $(x_v, y_v) = (-6.0, 0.26)$ and $(x_v, y_v) = (-5.5, 0.26)$ in Figs. 3a and 3b, respectively. The strength of the traveling vortex is $\Gamma_v = 0.2$ for both cases. The externally generated conservation of vorticity condition is used for both cases. It is seen that the present computed results and those of Wu et al. show a small dip in C_L as the vortex passes the trailing edge, whereas other results taper off thereon, showing no dip. According to our earlier interpretation of the C_L-dip phenomenon of Fig. 2, we believe that the no-dip results of Refs. 15 and 7 probably indicate an inadequacy in flow modeling of the Kutta condition. On the other hand, judging from the exact solution of Chow et al. in Fig. 2 and that of Renzoni and Mayle,[18] it is clear that the present results and Wu et al.'s results tend to be correct.

Impulsively Started Blade Pair

Figures 4–7 present eight different transient lift cases of an impulsively started blade pair, including their corresponding computed

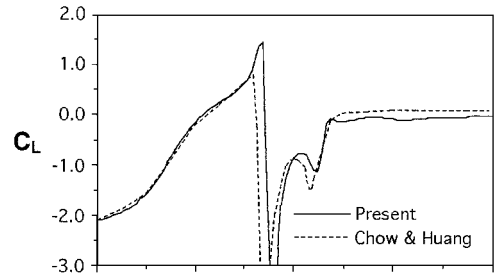

a) Lift coefficient

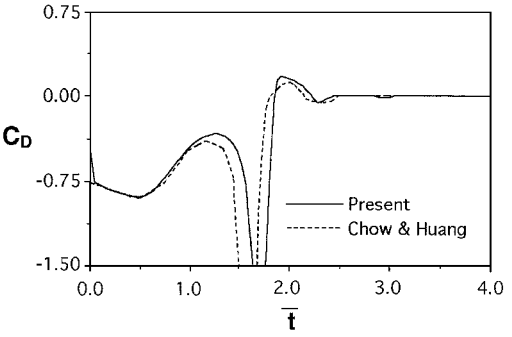

b) Drag coefficient

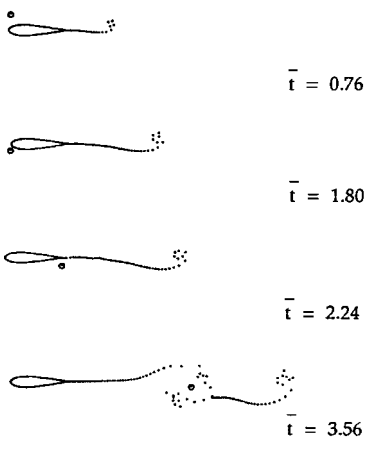

c) Wake patterns

Fig. 2 Traveling vortex over a 16.9% Joukowski airfoil (VAI); verification with the work of Chow and Huang.[6]

Table 1 Various parameters for studies of impulsively started blade pair: Figs. 4–7

Figure	τ,%	d/c	h/c	α, deg	C_{Ls} Front	C_{Ls} Rear
4a	2	2.0	0.0	5	0.70138	0.40793
4b	12	2.0	0.0	5	0.75733	0.42180
4c	2	2.0	1.0	5	0.68050	0.41991
4d	12	2.0	1.0	5	0.71304	0.43397
6a	2	0.0	0.5	5	0.40654	0.40063
6b	12	0.0	0.5	5	0.62069	0.21921
6c	12	1.5	0.2	5, 0	0.47540	−0.14086
6d	12	1.5	0.2	5	0.76485	0.38973

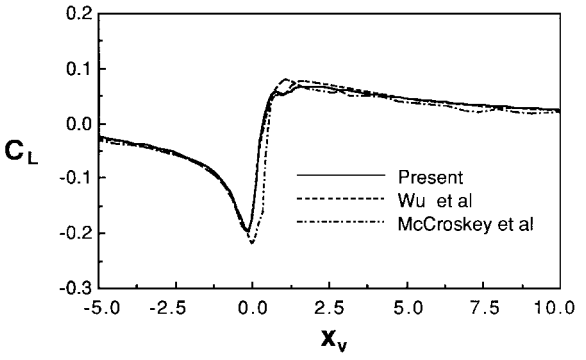

a) Verification with works of Wu et al.[14] and McCroskey and Goorjian[15]

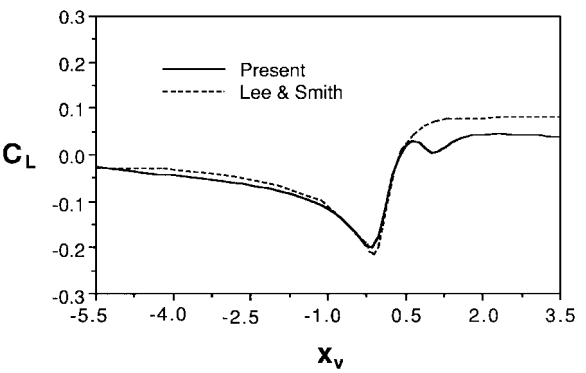

b) Verification with the work of Lee and Smith[7]

Fig. 3 Traveling vortex over a 12% Joukowski airfoil (VAI).

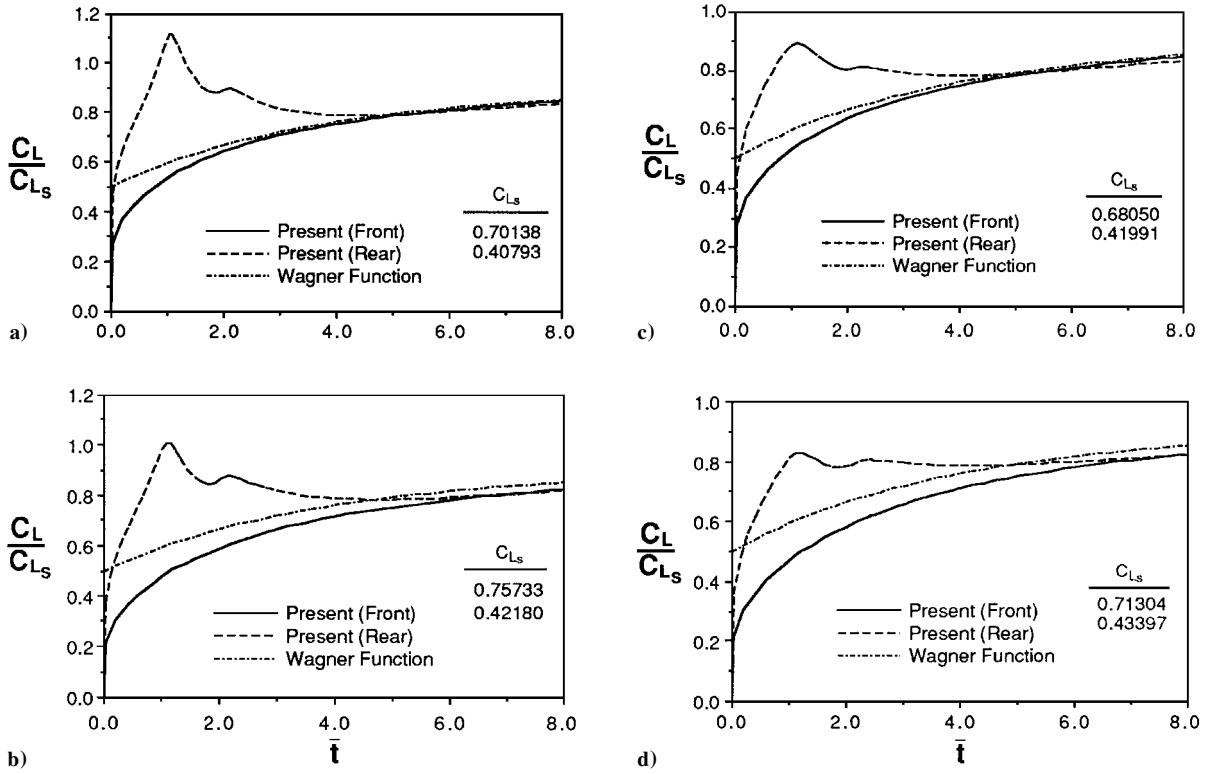

Fig. 4 Transient lifts of impulsively started blade pair (BBI): α = 5 deg and *d*/*c* = 2.0. Coplanar configurations: a) τ = 2.0% and *h*/*c* = 0.0 and b) τ = 12% and *h*/*c* = 0.0. Staggered configurations: c) τ = 2.0% and *h*/*c* = 1.0 and d) τ = 12% and *h*/*c* = 1.0.

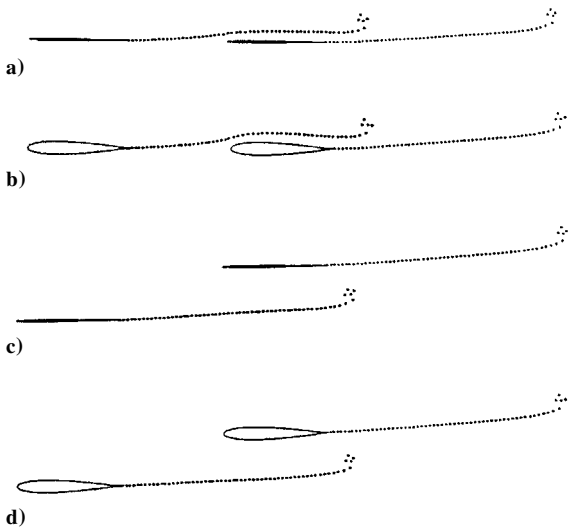

Fig. 5 Wake patterns corresponding to Figs. 4a–4d.

wake patterns. Various parameters such as airfoil thickness, blade distances, and steady lift coefficients for the front and the rear blades are listed in Table 1. In each case, the normalized transient lift coefficients (C_L/C_{L_s}) on the blades are plotted against the dimensionless time. Also shown are the associated wake patterns. All figures here present an impulsively started blade pair under three basic configuration arrangements: the coplanar, the staggered, and the unstaggered.

In Fig. 4 the humps and dips in the transient lift on the rear blade are seen in both the coplanar and the staggered cases. Clearly this is caused by the wake vortex interacting with the leading and trailing edges of the rear airfoil. For thinner airfoils with the coplanar arrangement, the transient lift becomes most peaky, and they can provide effective lift generation. In this case, the VAI at the leading edge is most pronounced as the wake vortex assumes the steepest trajectory in the proximity.

For a blade pair in impulsively started motion such as that of Fig. 4a, the rear blade could generate additional lift in excess to its steady lift. It is also observed that whether the oncoming wake vortices go above or below the rear blade, excessive lift can be generated on the blade until the main body of the wake vortices moves beyond several chords downstream. From this point onward, the lift generated by the blade system asymptotically converges to that of a single impulsively started airfoil, the lift according to Wagner's function[25] (Figs. 4a–4d). For unstaggered blades (Figs. 6a and 6b) the interaction is comparatively weak, and the lift generation of this system is not effective. Such an unsteady motion would be inferior to a stationary flow over the blade pair in terms of lift generation. The transient lift approaches asymptotically to its steady limit at a rather slow rate.

Figures 6c and 6d compare the computed results of transient lifts with those of Platzer et al.[24] Note that the presently defined impulsively started blade pair system as well as the built-in starting mechanism are different from those of Platzer et al.[24] The discrepancy found in Figs. 6c and 6d is likely to be caused by this difference in definition. Present definition strictly follows that of Wagner[25]; for example, in Fig. 6d both blades are kept at $\alpha = 5$ deg initially at rest and then impulsively accelerated to a given freestream speed. Platzer et al.'s definition adopts the indicial motion defined by Bisplinghoff et al.,[36] in which both blades are subject to a step change of angle of attack (from α = 0 to 5 deg) at an ongoing freestream speed. These two approaches should yield the same indicial aerodynamics for a single blade, but not so for two blade-pair systems defined differently. In particular, the rear blade would be subject to different transient flows in two systems at the initial state; however, this difference would vanish as the flows become steady. In Fig. 6d it can be seen that two transient lifts for both blades depart from each other initially and reach the same values asymptotically as the time goes on.

Pitching Blade Pair in Tandem

Figures 8–12 present two cases of a pitching coplanar blade pair in tandem. Case A is defined in Fig. 8 with the front blade in pitching motion about its midchord and the rear blade at rest; case B is defined with the blade arrangement in reverse order. Figure 9c shows the wake pattern during the first three cycles of the oscillation for case A. Computed results of case B are not shown here but can be found in Refs. 31 and 35. It is found that the movement of the wake vortices

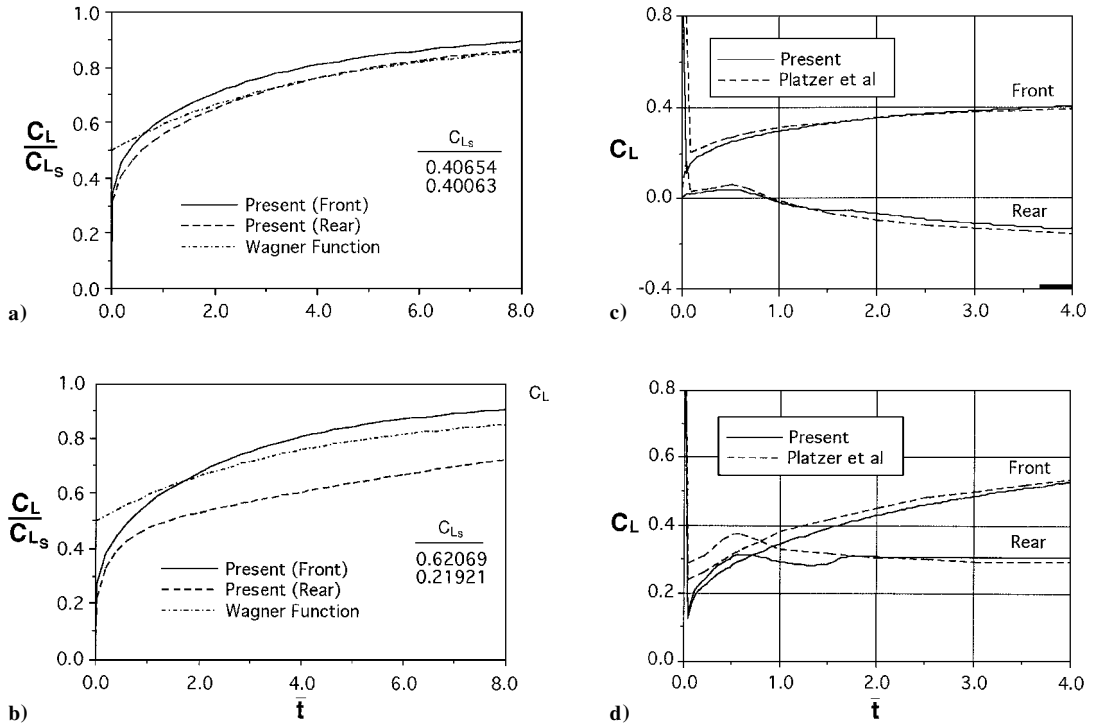

Fig. 6 Transient lifts of impulsively started blade pair (BBI): $\alpha = \alpha_{front} = 5.0$ deg. Unstaggered configurations: a) $\tau = 2.0\%$ and $h/c = 1.0$ and b) $\tau = 12\%$ and $h/c = 1.0$. Staggered configurations (verification with Platzer et al.[24]): c) $\alpha_{rear} = 0.0$ deg, $\tau = 12\%$, $d/c = 1.5$, and $h/c = 0.2$, and d) $\alpha_{rear} = 5.0$ deg, $\tau = 12\%$, $d/c = 1.5$, and $h/c = 0.2$.

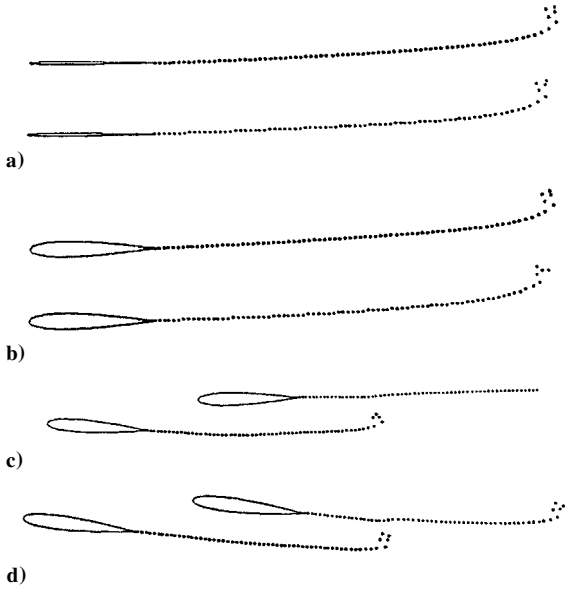

Fig. 7 Wake patterns corresponding to Figs. 6a–6d.

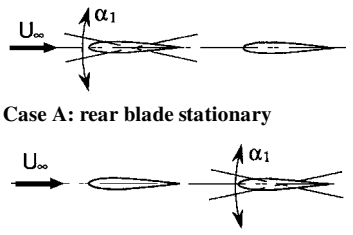

Fig. 8 Pitching blade pair in tandem (BBI).

on the rear blade for both cases are apparently different. Because the wake vortices provided in both cases are relatively weak ($\Gamma_v \sim 10^{-2}$), as opposed to the example shown for the VAI case ($\Gamma_v \sim 1.5$), the wake vortices as cut by the rear airfoil are expected to slide along its surface. Behind the rear blade, considerable wake–wake interaction can be seen for case A (but not so for case B). Toward the end of the third cycle in case A, two wakes begin to loop up, whereas no wake looping takes place in case B. In passing, it is noted that for a plunging counterpart of case A, even stronger wake looping activity is found in the wake patterns.[31]

Figures 9a and 9b show the lift and moment responses of the blade system (case A) due to a sinusoidal motion input of the front blade oscillating about its midchord at an amplitude of 1.0 deg and a reduced frequency of 4.0, respectively. Although the response of the front blade appears to be sinusoidal, that of the rear blade appears only to be periodic because it contains higher-order harmonics. The source of higher harmonics could be brought in from the vortex interaction and time integration scheme. Furthermore, it is interesting to observe that, whereas the well-developed response of the front blade occurs within the first cycle, that of the rear blade only begins at the third cycle.

Figure 10 presents the in-phase and out-of-phase lift and moment derivatives (called lifts and moments) for cases A and B, respectively. In Fig. 10, it can be seen that the lifts and moments of the rear blade are substantially affected by the impinging wake vortices throughout the frequency range, whereas those of the front blade remain essentially unaffected by the presence of the rear blade.

In the present study, computed results based on NACA0002 airfoils are found to be in good agreement with all of Bosch's[23] results based on flat plates for both cases A and B.

Schmidt's Wave Propeller

A novel propulsive machine known as the wave propeller was invented by Schmidt[28] during the 1940s. Shown in Fig. 11, Schmidt's wave propeller was claimed to reach 100% in its propulsive efficiency. To evaluate the thrust and efficiency of Schmidt's machine, Bosch[23] considered the oscillating flat plate model as shown in Fig. 12 using the kernel function approach. Here, the average drag coefficient and efficiency are defined according to Bosch,[23] i.e.,

$$\bar{C}_D = \frac{k}{2\pi}\int_0^{2\pi/k} C_D(t)\,\mathrm{d}t \tag{12}$$

and

$$\eta = \frac{\bar{D}U_\infty}{W}$$

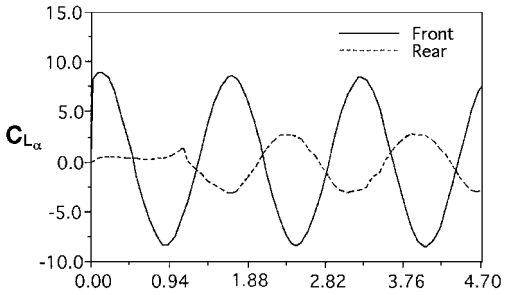

a) Lift histories of case A

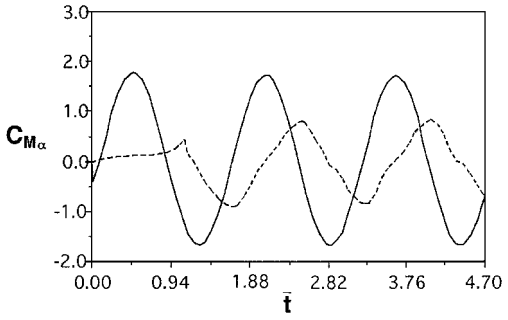

b) Moment histories of case A

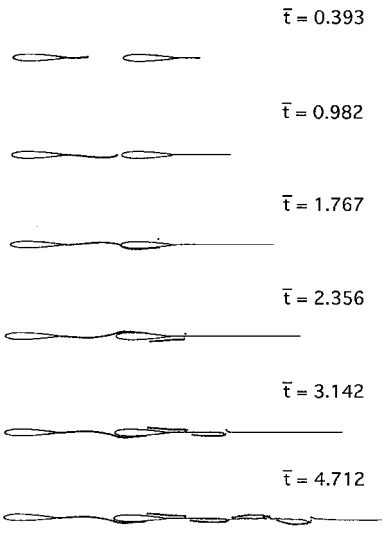

c) Wake patterns (front blade in pitching about its midchord: α_1 = 1.0 deg, τ = 2.0%, d/c = 2.0, and k = 4.0)

Fig. 9 Pitching blade pair in tandem (BBI).

where $\bar{D} = \bar{C}_D \times \frac{1}{2}\rho U_\infty^2 \cdot c$, and for an airfoil in pitching oscillation the averaged work done within one cycle amounts to $W = \frac{1}{4}\rho U_\infty^3 k\,\mathrm{Im}(C_M)$. Hence, for cases A and B, the averaged propulsive efficiency becomes

$$\eta = \frac{2\cdot\left[\left(\bar{C}_{D_{\alpha^2}}\right)_{\mathrm{Front}} + \left(\bar{C}_{D_{\alpha^2}}\right)_{\mathrm{Rear}}\right]}{k\cdot\mathrm{Im}\left(C_{M_\alpha}\right)} \tag{13}$$

In Fig. 12, the present computed results in $\bar{C}_D$ and η are verified with those obtained by Bosch.[23] Schmidt's machine corresponds to the arrangement of case A, which interestingly shows a drastic gain in thrust (negative $\bar{C}_D$) produced by the rear blade at the high-frequency end ($k = 4.0$). The propulsive efficiency indeed nearly approaches unity at $k = 4.0$. On the other hand, case B again is found ineffective in this respect.

For application of BBI to the preceding problem, it can be concluded that the major contribution of either the lift or the thrust forces are due to the wake–airfoil interaction such as those produced in case A. Unsteady airfoil interference effect does not appear to be notable in all cases considered here. Moreover, in case A, the rear blade converts the vortical energy generated by the pitching blade into additional thrust. The means to absorb this energy is through a proper arrangement of the transient induced velocity by the wake vortices.

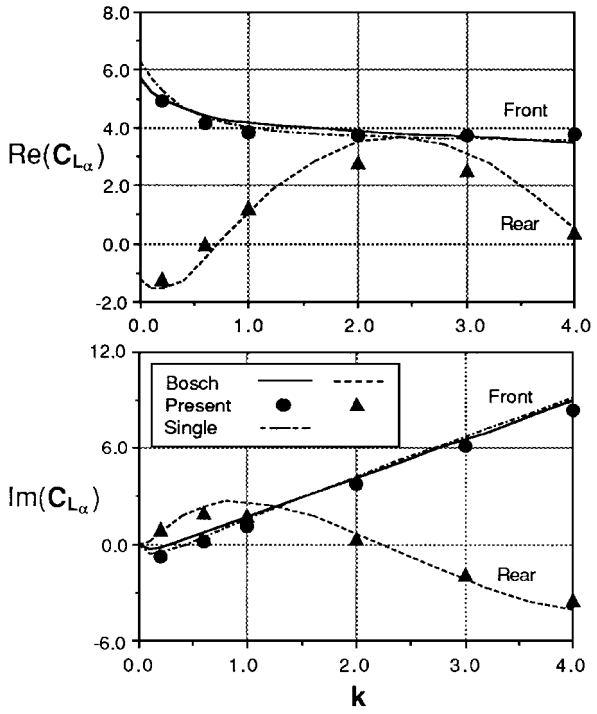

Lift derivatives vs reduced frequency

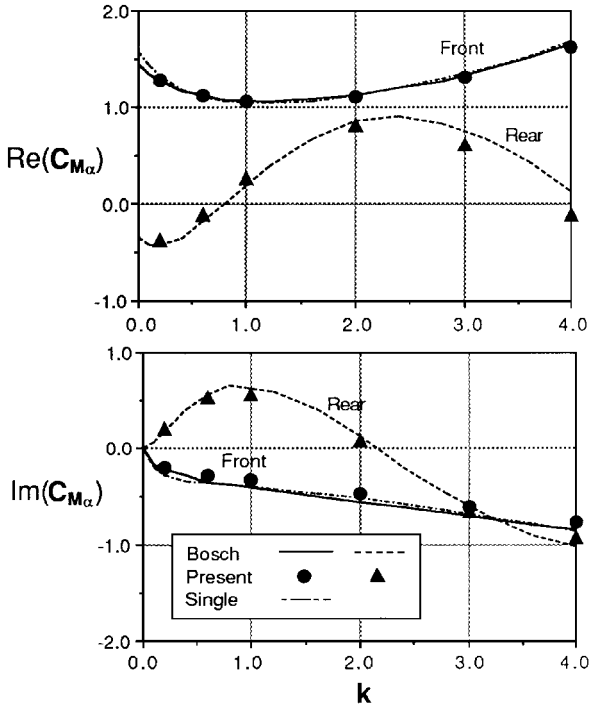

Moment derivatives vs reduced frequency

Fig. 10 Pitching blade pair in tandem (BBI). Verification with the work of Bosch[23] (front blade in pitching about its midchord: α_1 = 1.0 deg, τ = 2.0%, d/c = 2.0, and k = 4.0).

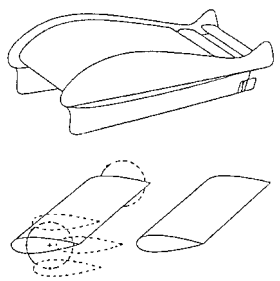

Fig. 11 Schmidt's wave propeller.

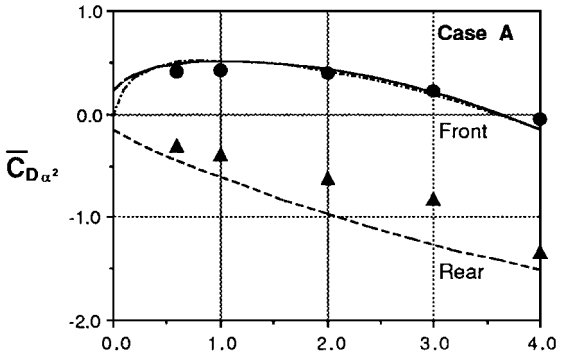

a) Average drag coefficients vs reduced frequency for case A

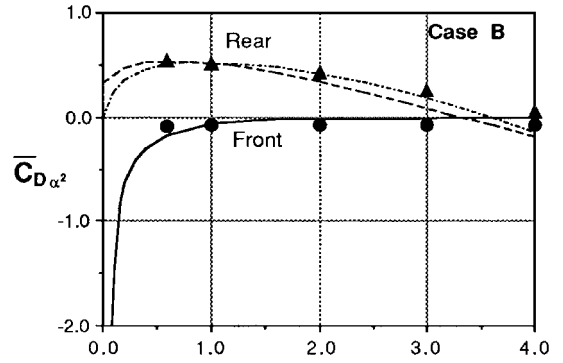

b) Average drag coefficients vs reduced frequency for case B

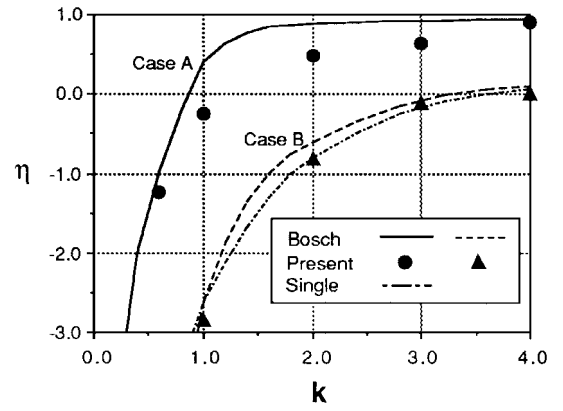

c) Propulsive efficiencies vs reduced frequency for cases A and B

Fig. 12 Pitching blade pair in tandem (BBI); verification with the work of Bosch.[23]

V. Conclusions

Several conclusions can be drawn based on the present studies of VAI and BBI problems.

1) A computed C_L dip appears when a traveling vortex or vortices passes by the lower side of the trailing edge, which judiciously reflects the proper flow modeling of the Kutta condition.

2) The present pitching blade pair study demonstrates that any front blade movement will result in a strong interaction between the wake and the rear blade, and thus it alters drastically the lift response of the latter (case A), whereas any rear blade movement remains ineffective in response, and thus it results in a weak interaction (case B).

3) For strong interaction cases, the coplanar arrangement is found to be most effective in the lift generation of the rear blade. Also, the same arrangement is found to be most effective to enhance the transient lift of the rear blade in the case of an impulsively started blade pair.

4) Strong interaction also results in a strong wake–wake interaction as shown by the wake-looping pattern of case A. No such pattern is observed in case B.

5) Bosch's previous finding on Schmidt's wave propeller is further generalized. A coplanar stationary blade behind a front blade in harmonic oscillation could produce considerable thrust, hence enhancing substantially the system propulsive efficiency. However, the thrust and the efficiency will decrease with increasing blade thickness.

Based on a general formulation, the present method is shown to handle a large class of problems in vortex dynamics and blade–blade interactions, a capability that is lacking in almost all previous methods. The vortex impingement condition as an option in the computing procedure further enhances the effectiveness and the robustness of the present method. Hence, the present method should be a basic tool in studying the generic VAI and BBI problems for the rotor–blade aerodynamics of turbomachinery and helicopters.

Acknowledgments

We thank Max Platzer and Kevin Jones of the U.S. Naval Postgraduate School for their critiques and suggestions in their review of the present paper. Invaluable discussions with Hernan Posnansky on the fundamentals of the present subject are gratefully appreciated.

References

[1] *Proceedings of U.S. Army Research Office Workshop on Blade-Vortex Interaction*, NASA Ames Research Center, Moffett Field, CA, Oct. 1984.

[2] Chorin, A. J., "Numerical Study of Slightly Viscous Flow," *Journal of Fluid Mechanics*, Vol. 57, Pt. 4, 1973, pp. 785–796.

[3] Giesing, J. P., "Nonlinear Two-Dimensional Unsteady Potential Flow with Lift," *Journal of Aircraft*, Vol. 5, No. 2, 1968, pp. 135–143.

[4] Basu, B. C., and Hancock, G. J., "The Unsteady Motion of a Two-Dimensional Airfoil in Incompressible Inviscid Flow," *Journal of Fluid Mechanics*, Vol. 87, Pt. 1, 1978, pp. 159–178.

[5] Kim, M. J., and Mook, D. T., "Application of Continuous Vorticity Panels to General Unsteady Incompressible Two-Dimensional Lifting Flows," *Journal of Aircraft*, Vol. 23, No. 6, 1986, pp. 464–471.

[6] Chow, C. Y., and Huang, M. K., "Unsteady Flows About a Joukowski Airfoil in the Presence of Moving Vortices," AIAA Paper 83-0129, Jan. 1983.

[7] Lee, D. J., and Smith, C. A., "Distortion of the Vortex Core During Blade/Vortex Interaction," AIAA Paper 87-1243, June 1987.

[8] Yao, Z. X., Garcia-Fogeda, P., Liu, D. D., and Shen, G., "Vortex/Wake Flow Studies for Airfoils in Unsteady Motions," AIAA Paper 89-2225, July–Aug. 1989.

[9] Katz, J., and Weihs, D., "Behavior of Vortex Wakes from Oscillating Airfoils," *Journal of Aircraft*, Vol. 15, No. 12, 1978, pp. 861–863.

[10] Choi, D. H., and Landweber, L., "Inviscid Analysis of Two-Dimensional Airfoils in Unsteady Motion Using Conformal Mapping," *AIAA Journal*, Vol. 28, No. 12, 1990, pp. 2025–2033.

[11] Rokhsaz, K., Selberg, B. P., and Eversman, W., "Effect of Thickness on the Unsteady Aerodynamics of Closely Coupled Oscillation Airfoils," *Journal of Aircraft*, Vol. 28, No. 8, 1991, pp. 312–319.

[12] Chow, C. Y., and Huang, M. K., "The Initial Lift and Drag of an Impulsively Started Airfoil of Finite Thickness," *Journal of Fluid Mechanics*, Vol. 118, May 1982, pp. 393–409.

[13] Sears, W. R., "Aerodynamics, Noise, and the Sonic Boom," *AIAA Journal*, Vol. 7, No. 4, 1969, pp. 577–586.

[14] Wu, J. C., Sankar, N. L., and Hsu, T. M., "Unsteady Aerodynamics of an Airfoil Encounter a Passing Vortex," AIAA Paper 85-0203, Jan. 1985.

[15] McCroskey, W. J., and Goorjian, P. M., "Interactions of Airfoils with Gust and Concentrated Vortices in Unsteady Transonic Flow," AIAA Paper 83-1691, July 1983.

[16] George, A. R., and Chang, S. B., "Flow Field and Acoustic of Two-Dimensional Transonic Blade-Vortex Interactions," AIAA Paper 84-2309, Oct. 1984.

[17] Caradonna, F. X., Strawn, R. C., and Bridgeman, J. O., "An Experimental and Computational Study of Rotor-Vortex Interactions," Fourteenth European Rotorcraft Forum, Paper 18, Milan, Italy, Sept. 1988.

[18] Renzoni, P., and Mayle, R. E., "Incremental Forces and Moment Coefficients for a Parallel Blade-Vortex Interaction," *AIAA Journal*, Vol. 29, No. 1, 1991, pp. 6–13.

[19] Poling, D. R., and Dadone, L., "Blade-Vortex Interaction," *AIAA Journal*, Vol. 27, No. 6, 1989, pp. 694–699.

[20] Panaras, A. G., "Numerical Modeling of Vortex/Airfoil Interaction," *AIAA Journal*, Vol. 25, No. 1, 1987, pp. 5–11.

[21] Nowak, M., "Interaction of Two Airfoils Oscillating Harmonically in an Incompressible Flow," *Fluid Dynamics Transactions*, edited by W. Fiszdon, P. Kucharczyk, and W. Prosnak, Vol. 3, Polish Academy of Sciences, Juvata, Poland, 1967, pp. 775–786.

[22] Giesing, J. P., "Nonlinear Interaction of Two Lifting Bodies in Arbitrary Unsteady Motion," *Journal of Basic Engineering*, Vol. 90, No. 3, 1968, pp. 387–394.

[23] Bosch, H., "Interfering Airfoils in Two-Dimensional Unsteady Incompressible Flow," Fluid Dynamics Panel Symposium, Ottawa, ON, Canada, CP-227, AGARD, Sept. 1977 (Paper 7).

[24]Platzer, M. F., Neace, K. S., and Pang, C. K., "Aerodynamic Analysis of Flapping Wing Propulsion," AIAA Paper 93-0484, Jan. 1993.
[25]Wagner, H., "Dynamischer Auftrieb vo Tragflügeln," *Zeitschrift fuer Angewandte Mathematik und Mechanik*, Vol. 5, No. 1, 1925, p. 17.
[26]Theodorsen, T., "General Theory of Aerodynamic Instability and the Mechanism of Flutter," NACA Rept. 496, 1935.
[27]Katz, J., and Maskew, B., "Unsteady Low-Speed Aerodynamic Model for Complete Aircraft Configurations," AIAA Paper 86-2180, Aug. 1986.
[28]Schmidt, W., "Der Wellpropeller, ein neuer Antrieb für Wasser-, Land- und Luftfahrzeuge," *Zeitschrift für Flugwissenschaften*, Vol. 13, 1965, pp. 472–479.
[29]Kellogg, O. D., *Foundations of Potential Theory*, Dover, New York, 1952, p. 129.
[30]Batchelor, G. K., *An Introduction to Fluid Dynamics*, Cambridge Univ. Press, London, 1967, p. 273.
[31]Yao, Z. X., "Unsteady Aerodynamics of Blade-Blade Interactions," Ph.D. Thesis, Dept. of Mechanical and Aerospace Engineering, Arizona State Univ., Tempe, AZ, 1993.
[32]Shen, C. C., and Proft, E., "An Accurate Method for Calculation of Potential Flows About Arbitrary Airfoils," Northrop Corp., NOR 80-174, Hawthorne, CA, Dec. 1980.
[33]Morino, L., and Kuo, C. C., "Subsonic Potential Aerodynamics for Complex Configurations—A General Theory," *AIAA Journal*, Vol. 12, No. 2, 1974, pp. 191–197.
[34]Carnaham, B., Luther, H. A., and Wilkes, J. O., *Applied Numerical Methods*, Wiley, New York, 1969, p. 344.
[35]Yao, Z. X., and Liu, D. D., "Vortex Dynamics of Blade-Blade Interaction," AIAA Paper 94-0737, Jan. 1994.
[36]Bisplinghoff, R. L., Ashley, H., and Halfman, R. L., *Aeroelasticity*, Addison–Wesley, Cambridge, MA, 1955.

S. Fleeter
Associate Editor